Journal of Food Engineering 290 (2021) 110150

Contents lists available at ScienceDirect

Journal of Food Engineering

journal homepage: http://www.elsevier.com/locate/jfoodeng

In-situ rheological and structural characterization of milk foams in a commercial foaming device

Annika R. Völp [a,*], Lisa Kagerbauer [a], Jan Engmann [b], Deniz Z. Gunes [b], Cécile Gehin-Delval [c], Norbert Willenbacher [a]

[a] Institute for Mechanical Process Engineering and Mechanics: Applied Mechanics, Karlsruhe Institute of Technology, Switzerland
[b] Nestlé Research Center, Institute of Material Sciences, Vers-chez-les-Blanc, CH-1000, Lausanne, 26, Switzerland
[c] Société des Produits Nestlé SA, Nestlé Product Technology Center Beverage. Route de Chavornay 3, CH-1350, Orbe, Switzerland

ARTICLE INFO

Keywords:
Milk foam
Foam rheology
Bubble size distribution
In-situ rheometer geometry
Yield stress gradients

ABSTRACT

Processing, stability and sensorial perception of food foams are tightly related to their microstructure and flow behavior. Characterization of corresponding physical parameters is central for product development and quality control. An experimental setup enabling in-situ characterization of yield stress, gas volume fraction and bubble size distribution at different heights within a foam column created in a commercial whipping device is presented. Reliable determination of these quantities is shown. Foams made from regular and reconstituted milk have been investigated. Gas volume fraction and bubble size increase monotonically during free drainage. Related to the changes in these parameters, the yield stress increases strongly during initial drainage and weaker in mature foams. Gradients of the structural and rheological parameters along the direction of gravity increase over time. Yield stresses in these milk foams are as predicted from phenomenological modelling including the above parameters, emphasizing the reliability of the measurement setup.

1. Introduction

Coffee is the most popular hot beverage among Europeans, who consume about 2.5 million kg coffee beans annually (ICO, n. d.). Milk foam is added to every second coffee served in German and Austrian gastronomy (AMA Marketing, n. d.; Statista, n. d.). Latte and cappuccino varieties are also the most popular coffee products purchased in the UK (Worldpanel, n. d.). The variety of coffee specialties based on milk foams has long gone beyond cappuccino and latte macchiato, and new coffee trends for instance in latte art, the creation of decorative patterns by pouring microfoam into coffee, push the development of foaming devices and recipes for foaming solutions based on dairy products or vegan replacements. Milk based food foam products with a broad range of rheological behavior are available serving manifold applications and ideally providing pleasant texture perception. Tailoring their stability and flow behavior remains a challenge for the food industry (Gunes D. Z., Engmann J., Gehin-Delval C., Schmitt C., 2018). The flow behavior is strongly related to micro-structural properties, mainly bubble size distribution and gas volume fraction, which are often subject to local inhomogeneity within a foam column and difficult to predict for complex food systems.

In foams under gravity, a vertical gradient in gas volume fraction develops due to drainage of the liquid fraction. The gas volume fraction can range between almost 100% at the foam top and less than 64% at the foam bottom. The latter is the critical gas volume fraction of random close packing of monodisperse, spherical bubbles. For polydisperse bubble size distributions, this critical gas volume fraction is higher (Lexis and Willenbacher, 2014; Farr and Groot, 2009). Below the critical packing fraction, foams behave like purely viscous fluids unless there are attractive interactions among the species stabilizing the bubble interfaces (Cohen-Addad and Höhler, 2014; Saint-Jalmes and Durian, 1999). Foams with gas volume fraction exceeding the critical volume fraction exhibit elastic behavior under small shear stresses and a critical stress, also termed yield stress, at which bubble rearrangements enable onset of foam flow. For complex fluids such as milk foams, the true deformation field within a sample is often not known. The critical stress at which the apparent deformation or flow rate in a rheometer increases drastically is called apparent yield stress. The elastic modulus and the yield stress scale with the "Laplace pressure" inside the bubbles, given by the ratio between surface tension and the Sauter bubble radius, the foams gas volume fraction and the maximum packing fraction referring

* Corresponding author.
E-mail addresses: annika.voelp@kit.edu (A.R. Völp), norbert.willenbacher@kit.edu (N. Willenbacher).

https://doi.org/10.1016/j.jfoodeng.2020.110150
Received 25 November 2019; Received in revised form 14 May 2020; Accepted 21 May 2020
Available online 7 June 2020

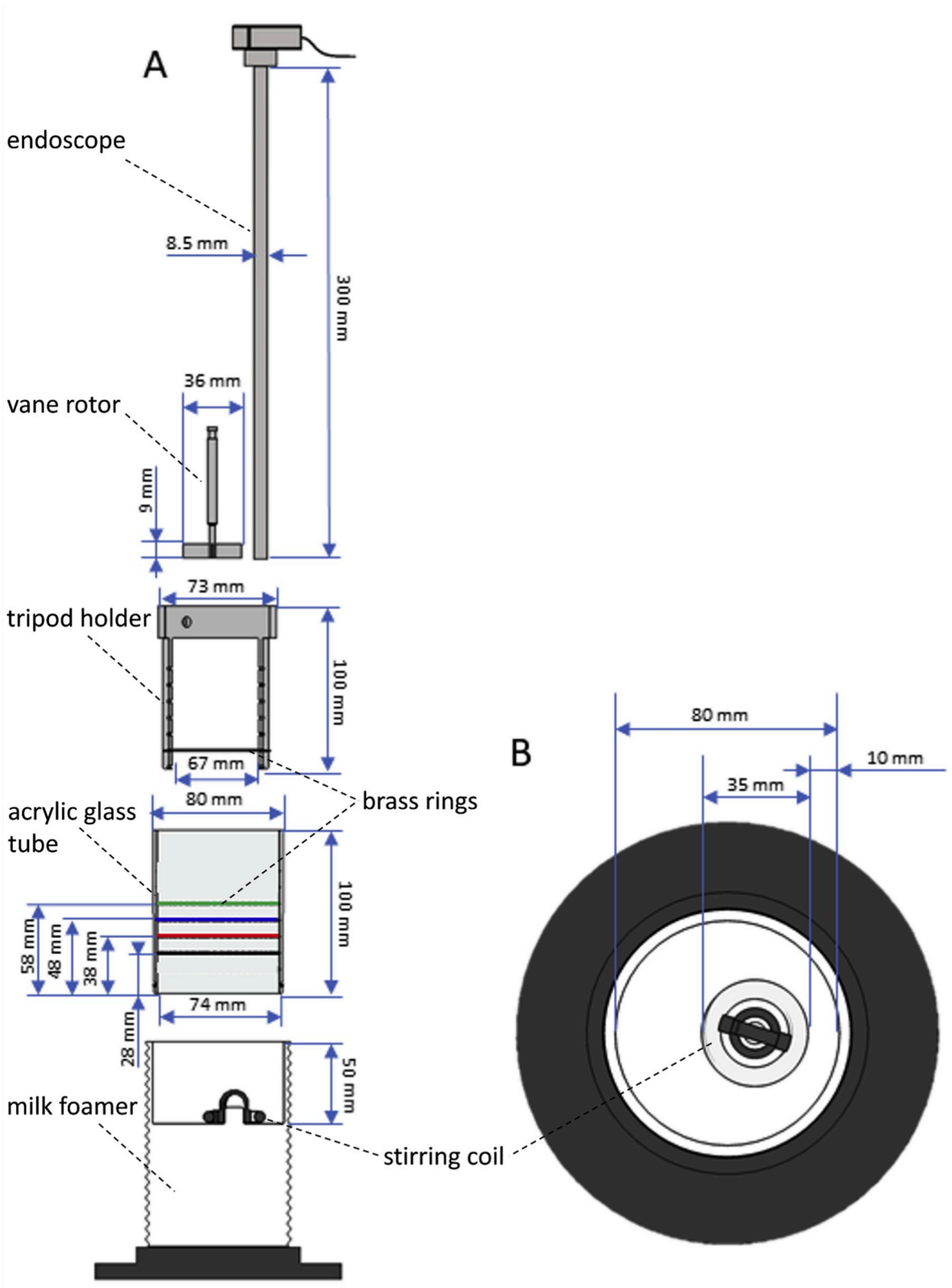

Fig. 1. Modified commercial milk foamer (Nespresso Aeroccino4) for in-situ determination of gas volume fraction, yield stress and bubble size at various foam heights in side view (A) and top view (B) of the foamer.

to the particular bubble size distribution (Marze et al., 2005; Mason et al., 1996). A vertical gradient in gas volume fraction develops with foam age and as a consequence, coalescence and hence the bubble size distribution alters along the vertical axis. These structural changes also result in a gradient of foam rheological properties within the foam column. To characterize the spatial and temporal changes of foam structure and rheology, a methodology allowing for unperturbed foam aging and in-situ characterization is needed.

We have developed an experimental setup, which allows for the characterization of milk foam rheological and micro-structural

properties at different heights along a foam column within a commercial whipper. The cylindrical container with eccentric whipping coil and heating plate at the bottom is built into a rotational rheometer. Yield stresses are measured with a vane rotor at regular intervals along the rotational axis of the container. Bubble size distributions are analyzed via endoscopic imaging and automated bubble detection at the same heights with temporal resolution on the order of seconds. Gas volume fractions are obtained from electrical conductivity measurements. Brass rings at the inner container wall and a height adjustable ring submerged into the foam serve as electrodes to detect the conductivity at intervals along the vertical axis.

Results presented for different types of milk foams confirm the feasibility of the device, provide some new insight regarding microstructure and flow of such foams and may contribute to design optimization of commercial food foaming devices.

2. Materials and methods

2.1. Modification of the foaming device

Fig. 1 shows the setup developed for the in-situ characterization of the milk foams. It consists of a modified commercial milk foamer (Nespresso Aeroccino 4, Nespresso S.A., Lausanne, Switzerland), an acrylic glass tube fitted with conductivity electrodes, an endoscope and a vane rotor.

The top of a commercial milk foamer consisting of a pourer and a handle was replaced by an acrylic glass tube (Evonik Plexiglass, 100 mm height, 80 mm outer diameter, 74 mm inner diameter). Customized brass rings (1 mm height, 76 mm outer diameter, 74 mm inner diameter) were flush-mounted to the inner wall of the acrylic glass tube at 28, 38, 48 and 58 mm height (with respective 1 mm holes for electrode connections at each height). Another customized brass ring (1 mm height, 69 mm outer diameter, 67 mm inner diameter) was fixed to a tripod holder (3D printed, 100 mm height, 73 mm outer diameter, 67 mm inner diameter, co-polyester based material: Colorfab xt, Belfeld, Netherlands). The tripod holder was designed to place the brass ring at the heights of 28, 38, 48 and 58 mm, opposite to the brass rings mounted in the acrylic glass tube. This allowed for measuring the foam conductivity at four different heights inside the foamer. To conduct the rheometric measurements, the foamer was centered into a rheometer mounting plate using an annular spring clamp (Ringfeder, RfN 8006, 8 cm inner diameter). A four bladed vane of 36 mm in diameter and 9 mm in height, was manufactured for measuring foam yield stress.

2.2. Sample preparation

Reconstituted milk was prepared by dispersing 15 g of a commercially produced milk powder (provided via Nestlé Research, Switzerland) in 120 ml of mineral water (Vittel® containing 255.7 mg/L monovalent ions and 234 mg/L divalent ions, Nestlé, Switzerland) during stirring for 70–80 s. An amount of 120 ml of either ultra-high temperature processed (UHT) whole milk (Alpenmich, haltbar, 3.5% Fett, Alnatura, Bickenbach, Germany), fat reduced UHT milk (Alpenmich, haltbar, 1.5% Fett, Alnatura, Bickenbach, Germany) or reconstituted milk at room temperature was filled into the foamer. The milk was whipped using the stirring coil eccentrically placed at the bottom of the foamer as depicted in Fig. 1B. During whipping, the temperature was increased with a rate of 0.6 °C/s via heating through the bottom of the foamer's cell. The foaming process stopped after approximately 70 s when the temperature of the milk at the bottom inside the foamer had reached 60 °C. All measurements started after the foaming process had stopped. The nutrition information of the UHT milk and the solution of 12.5% milk powder, as specified by the manufacturer, and the surface tension, measured as described in section 2.3, are given in Table 1.

Table 1
Compositional information (in weight %) and surface tension of whole milk, fat reduced milk and reconstituted milk made of 12.5% milk powder.

	UHT whole milk	UHT fat reduces milk	12.5% reconstituted milk
Fat	3.6%	1.6%	3.6%
Carbohydrates	5%	5.1%	3.2%
Proteins	3.3%	3.4%	3.4%
Salt	0.11%	0.11%	–
Surface tension	45.3 ± 0.1 mN/m	45.5 ± 0.2 mN/m	45.8 ± 0.6 mN/m

2.3. Surface tension determined using de Noüy ring

The surface tension Γ of the milk samples was determined using a tensiometer (DCAT11, DataPhysics Instruments) equipped with a platinum de Noüy ring (RG 11 - Du Noüy ring, DataPhysics Instruments, Filderstadt, Germany) with 25 mm height, 18.7 mm diameter and, 0.37 mm wire thickness (Lykema, J., Fleer, G. J., Kleijn, J. M., Leermakers, F. A. M., Norde, W., & Van Vliet, 2000).

2.4. Bubble size distribution determined using endoscopy

A non-flexible 295 mm long endoscope (TVS80.280. BF6. 10 CE.2x-Zoom, Visitool, Maulbronn, Germany) with a diameter of 8 mm was covered by an outer metal tube, 300 mm in length and 8.5 mm in diameter, closed with an optical glass disk (custom-made product, Visitool, Maulbronn, Germany) and was connected to a USB camera (Lumenera LU 160, Teledyne Lumenera, Ottawa, Kanada). The size to pixel ratio was determined by scaling the image of millimeter scaling paper held flat onto the glass disk of the endoscope covering tube. Subsequently, the endoscope was placed into the foamer with a distance to the bottom wall of 28, 38, 48 or 58 mm. The light outlets of a two-branched gooseneck lamp (KL 1500 LCD, Schott, Mainz, Germany) were placed inside the foamer pointing from opposite sites into the direction of the endoscope tip. The foamer was filled with 120 ml of sample and the foaming process was started. Once the foam covered the endoscope tip, the light intensity was adjusted between 0 and 600 lm to obtain even illumination of the foam. Images were recorded every 10 s starting immediately after the foaming process stopped. The images were analyzed using a template matching tool written in MATLAB® (Mathworks, Natick, USA) with 25 circular templates differing in diameter as described elsewhere (Völp and Willenbacher, 'unpublished results). The diameters were logarithmically distributed in the range between 10 and 250 pixels. The frequency density distribution histogram and the cumulative distribution of the bubble diameter counts and volumes were calculated from the obtained bubble size lists based on the 25 size classes. The span of the count distribution $(d_{90}\text{-}d_{10})/d_{50}$ and the Sauter radius r_{32} were calculated from the size distribution. All measurements were repeated at least three times with freshly prepared foams. The average and standard deviation of the counts and volumes for each size class, the span and the Sauter radius were calculated from bubble sizes lists deriving from three images of independently prepared foams at the same age. For validation of the automated bubble detection, the sum of all bubbles in three images of independently created foams, recorded after 300 s of drainage were additionally analyzed manually by three individuals who measured the bubble diameters. The bubble diameter counts and volumes for the same 25 size classes as above were obtained and their average and standard deviation referring to the analysis of the three individuals were calculated.

2.5. Gas volume fraction determined using electrical conductivity measurements

The conductivity κ of the foams between brass rings at the inner wall of the foamer with a distance to the bottom of 28, 38, 48 and 58 mm and the height adjustable ring with 5 mm smaller radius was measured and recorded using an LCR meter (U1733C 20,000-Count-Display Handheld

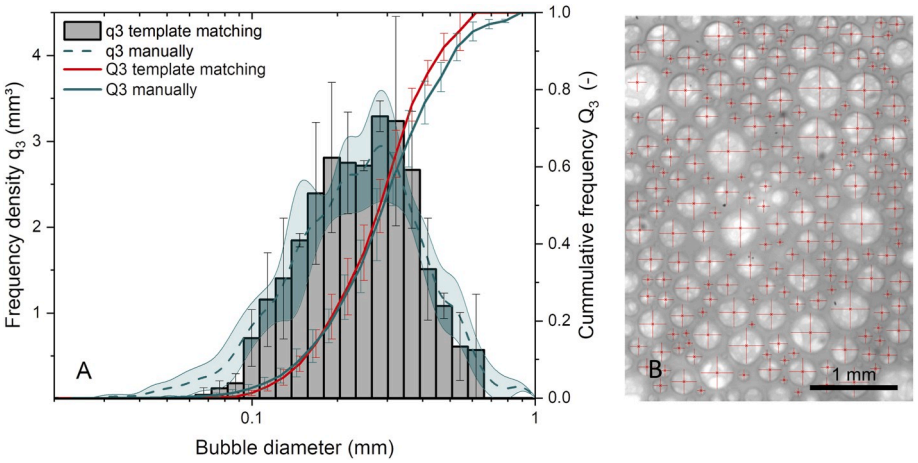

Fig. 2. Bubble size frequency density histogram and cumulative frequency distribution of bubble volumes analyzed using an automated template matching code (grey bars and solid red line) and manually by three individuals (dashed and solid green line) in endoscopic images of 12.5% reconstituted milk foam at 85% gas volume fraction (A). Red crosses mark the automatically detected bubble diameters in one of three images analyzed (B).

LCR Meter, Keysight Technologies, Santa Rosa, USA) with a test frequency set to 1 kHz. Beforehand, the setup was calibrated using potassium chloride solutions with conductivities between 10 and 10,000 μS/cm at 20°C. A cell-constant of 0.07/cm was determined. Using this cell-constant, the conductivities of potassium chloride solutions between 10^{-4} and 0.1 mol/l measured with the ring setup agreed reasonably with the conductivities measured using a commercial conductivity meter (S230 seven compact, Mettler Toledo, Schwerzenbach, Schweiz) equipped with a four-electrode conductivity sensor (Inlab® 738 ISM, Mettler Toledo, Schwerzenbach, Schweiz), as shown in Fig. A1.

Before foaming, the inner ring was placed at the height of interest opposite the outer ring and the LCR meter was connected to the copper cables attached to the brass rings. The foamer was filled with 120 ml of sample and the foaming process was started. The conductivity was measured immediately after the foaming process stopped and repeated at least three times with independently produced foam samples. For comparison, the conductivity was measured using the commercial conductivity probe equipped with a temperature sensor. The conductivity sensor of the commercial probe was placed in the foamer with a distance to the bottom wall of 28, 38, 48 and 58 cm, respectively. Conductivity and temperature were recorded every 10 s.

The foam gas volume fraction φ was calculated using following empirical correlation (Feitosa et al., 2005):

$$\varphi = 1 - \left(3\ \kappa_{rel.} + 33\ \kappa_{rel}\right)/(1 + 25\ \kappa_{rel} + 10\ \kappa_{rel})^2 \quad (1)$$

where κ_{rel} is the foam conductivity relative to the milk conductivity at 25 °C, respectively

$$\kappa_{rel.} = \kappa_{foam}(25^{\circ}C) \,/\, \kappa_{milk}(25^{\circ}C). \quad (2)$$

Beforehand, the foam conductivity at 25 °C, $\kappa_{foam}(25°C)$, was calculated from the conductivity measured at temperature T using a linear temperature correction (Zhang, 2007):

$$\kappa(25^{\circ}C) = \kappa_{foam}(T) \,/\, (1 - \alpha(25^{\circ} - T)) \quad (3)$$

where $\kappa_{foam}(T)$ is the foam conductivity at the foam temperature T and α is the temperature correction factor. The conductivity and temperature of the milk sample was measured during temperature decay to room temperature to obtain α from the slope of the milk conductivity versus temperature $\Delta\kappa_{milk}/\Delta T$ and the milk conductivity at 25 °C, $\kappa_{milk}(25°C)$:

$$\alpha = (\Delta\kappa_{milk}/\Delta T)/\kappa_{milk}(25^{\circ}C) \quad (4)$$

For comparison, the gas volume fraction was also determined from volumetric measurements. The entire content of the foamer was poured into a measuring cylinder of 250 ml capacity directly after foaming 120 ml of milk. The volume of the foam V_{foam} and the drained milk V_{milk} was captured at 15, 30, 60, 120, 180, 240, 300 and 600 s of foam age. The gas volume fraction was calculated as follows:

$$\phi = 1 - (120\ ml - V_{milk}) \,/\, V_{foam} \quad (5)$$

2.6. Foams' yield stress determined using a vane Rheometer

A rotational rheometer (Mars II, Haake Thermo Fisher Scientific, Karlsruhe, Germany) with an in-house manufactured, four bladed vane rotor (36 mm diameter, 9 mm height) and the foamer built into the rheometer as measuring cup was used. For yield stress measurements, the foam samples were prepared in the foamer. Then the vane geometry was lowered to the measuring position in the foam. The measurement was started when the foam reached the desired foam age. For reference, a rotational rheometer (Rheoscope1, Haake Thermo Fisher Scientific, Karlsruhe, Germany) and a plate-plate geometry 60 mm in diameter was used. Bottom plate and rotor plate were covered with sandpaper (grit 40, average particle diameter 269 μm) to reduce wall slip effects. The required foam volume was approximately 20 ml. The gap height was set to 6 mm. A foam sample was prepared inside the foamer. A scoop of foam was withdrawn from the foamer using a spoon and was put onto the bottom plate 20 s before it reached the desired foam age and the measurement was immediately started. The device set the gap automatically within 20 s.

In both cases, shear stress σ was increased from 0.1 to 50 Pa in 12 logarithmically distributed steps during a total measuring time of 60 s. The measurement was repeated at least three times with freshly prepared foam samples. The recorded deformation γ was plotted versus shear stress logarithmically and the yield stress σ_y was determined using the tangent intersection point method as described elsewhere (Willenbacher and Lexis, 2018).

For validation of the measurements using the in-house manufactured vane, the yield stresses of commercial o/w- and w/o-emulsion (Nivea Soft and Nivea Body Milk, Beiersdorf, Hamburg, Germany) were measured with the vane geometry and with a plate-plate geometry (60 mm in diameter covered with sand paper and 5 mm gap height). After the measuring positions of the vane rotor or upper plate was set, samples were left to rest for at least 15 min before measurements started. Shear stress was increased stepwise between 5 and 500 Pa in 20 logarithmically distributed steps for the o/w-emulsion and between 1 and 20 Pa in 15 logarithmically distributed steps for the w/o-emulsion solution. Measurements were repeated three times with every emulsion, respectively.

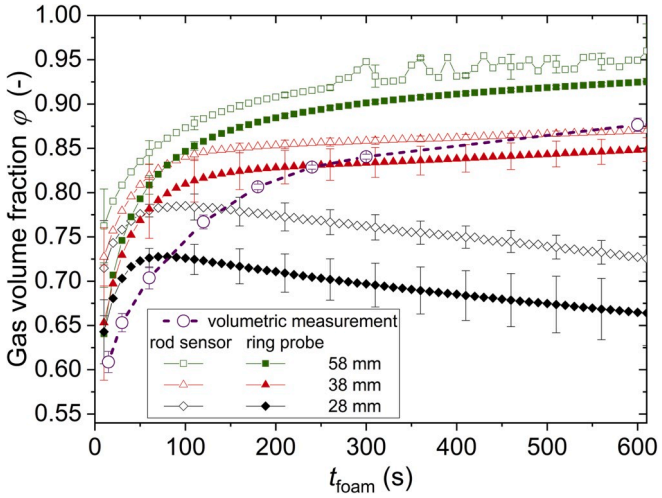

Fig. 3. Gas volume fraction φ versus foam age t_{foam} for 3.6% fat UHT milk foam measured in situ with commercial conductivity sensor (empty symbols) and brass ring electrodes (filled symbols) at three different heights inside the foaming device. Gas volume fraction of the entire foam, determined measuring ex-situ volumes of foam and drained milk, are also shown for comparison (open circles).

3. Results and discussion

3.1. Validation and performance of the foam characterization methods

Endoscopic foam images were analyzed to obtain the bubble size distribution. The images were acquired in the center of the milk foamer to avoid capturing bubbles distorted at the container wall. To validate the automated bubble size distribution approach, images of three milk foams at 85% gas volume fraction were recorded and analyzed both manually and using the template matching tool. During the manual data evaluation, approximately 700 bubbles in three images were analyzed by three individuals. Then, each image was analyzed using template matching. Fig. 2 shows an exemplary endoscopic image of the foam, wherein red crosses highlight the automatically detected bubbles. Fig. 2 also shows a comparison of the frequency density histograms and cumulative volume distributions obtained from manual analysis and template matching method, respectively. The automated analysis delivers the same results as the manual analysis up to a cumulative volume of 90%. The deviation above this value is caused by the fact that bubbles with diameters above 680 μm were not detected using the template matching method because of their lack in sphericity. These bubbles, however, were included in the manual analysis.

In-situ electrical conductivity measurements were performed at different heights within the foaming cell using brass ring electrodes as described above. Fig. 3 shows the time evolution of the gas volume fraction of a milk foam determined from conductivity measurements at different heights and compares them to those measured using a commercial conductivity sensor positioned at the same height. The foam gas volume fraction obtained with the ring electrodes are shifted to slightly lower values than obtained using the commercial conductivity sensor at 38 mm and 58 mm height inside the foamer. This systematic deviation is somewhat more pronounced at the height of 28 mm since it increases with increasing absolute value of conductivity and it is also found in simple salt solutions (Fig. A1). Despite the systematic deviations regarding the absolute gas volume fraction values, the time evolution captured with both methods is similar at all investigated foam heights. In the upper foam regions, drainage results in a monotonic increase of the gas volume fraction over time. However, close to the foam bottom at a height of 28 mm, the gas volume fraction goes through a maximum and then drastically decreases because of accumulation of drained liquid. The conductivity obtained with the commercial conductivity sensor tends to scatter in the dry limit of the foam resulting in unsteady gas volume fraction as seen for instance at the foam top, at 58 mm height, after 300 s foam age. Because of a ten times higher gap volume, the developed ring electrode setup seems to provide more robust conductivity measurements and hence more reliable gas volume fraction data. Finally, Fig. 3 also shows the time dependence of the volumetrically determined average gas volume fraction. These values lie in the same range as the in situ determined values in the middle of the foam column and exhibit the expected drainage-induced monotonic increase of the gas volume fraction over time.

Yield stresses σ_y of commercial o/w- and w/o-emulsions (Nivea Soft and Nivea Body Milk, Beiersdorf, Hamburg, Germany) measured with our customized vane geometry were validated using a rheometer equipped with a plate-plate geometry. Comparison of the corresponding data given in Table 2 demonstrates that the yield stress values measured using the short vane customized for in-situ foam characterization agree very well with those determined using the plate-plate geometry as well as with literature data.

The in-situ method allows the foams' yield stress to be measured along the vertical axis of the foamer with a resolution of 1 cm. Fig. 4 shows the time evolution of the yield stress during aging measured in situ at different heights directly inside the foamer and corresponding ex-situ values obtained using the plate-plate geometry. For all heights, the yield stress increases within the first 300 s and levels off to plateaus later on. The plateau value increases with height inside the foam column. These measurements exhibit a relative standard deviation of maximum 10%. Thus, the yield stress gradient within the foam can be well resolved using the in-situ measurement with the vane rotor. For measuring the yield stress ex situ with plate-plate geometry, as described earlier (Lexis and Willenbacher, 2014), approx. 20 ml of foam were transferred from the foamer into the fixture. As can be seen from Fig. 4, the value obtained for the yield stress from plate-plate rheometry agrees with data obtained in situ using the vane geometry only for young foams within the first minutes after their preparation. For older foams, yield stress

Table 2
Yield stress values of commercial emulsions obtained from vane and plate-plate rheometry, and literature.

Yield stress from	Vane	Plate-plate	Literature (Martinie et al., 2013)
o/w-emulsion Nivea Body Milk	10.9 ± 0.5 Pa	12.2 ± 0.7 Pa	8 Pa
w/o-emulsion Nivea Soft	91.0 ± 9 Pa	98.0 ± 18 Pa	91 Pa

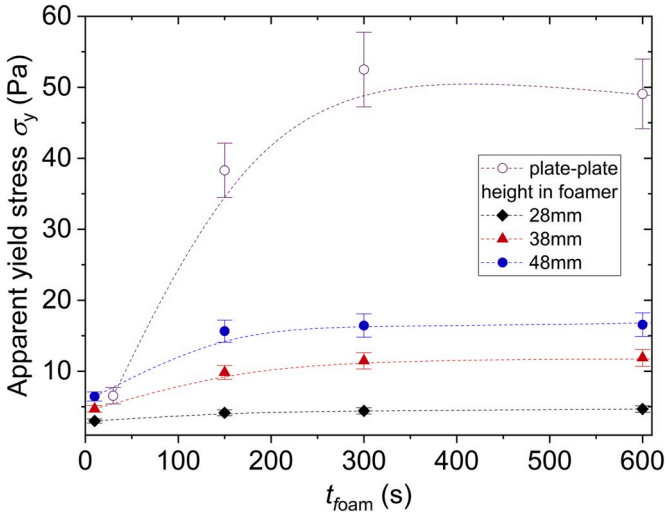

Fig. 4. Apparent yield stress σ_y versus foam age t_{foam} for 3.6% fat UHT milk foam measured ex situ with a plate-plate rheometer (empty symbols) and in situ with a vane rotor at three different heights inside the foaming device (filled symbols). Lines guide the eye.

values obtained using plate-plate geometry are at least three times higher than those determined in situ. Since deviations between yield stress data obtained using the customized short vane geometry and the commercial plate-plate fixture occur only in foams and not in commercial o/w- and w/o-emulsions (Table 2), we conclude that the latter data have a significant systematic error and we attribute this to the compression of the foam during gap setting. In young foams with low gas volume fraction, the compression does not lead to a significant change in bubble packing, presumably due to its narrow size distribution. Hence, no increase of the yield stress compared to the values obtained with the less invasive vane rotor were observed.

3.2. Structure and rheology of milk foams

We have used the experimental setup described and validated above to investigate the time evolution of the yield stress, gas volume fraction and bubble size distribution at different heights within the foam column created using the commercial whipper with its defined coil rotational speed and heating profile. Measurements have been performed for UHT whole milk, UHT fat reduced and reconstituted milk (see sec.2.1).

The time evolution of levels of the milk/foam-interface (filled symbols) and the foam/air-interface (open symbols) inside the foamer for reconstituted and for UHT milk with 1.6% fat and 3.6% fat is shown in Fig. 5. The foam volume is specific to the respective milk types and the foaming device used here, and was smallest in the case of 1.6% fat UHT milk. The foam collapse rates, seen in the decay of the upper foam limit, are similar for all foams investigated. The volume of non-foamed milk below the foam layer is initially highest after whipping 1.6% fat UHT milk and lowest after whipping 3.6% fat UHT milk. With ongoing drainage, the height of non-foamed milk approaches 25 mm inside the foamer (corresponding to a volume of 100 ml) in all cases. Measurements in the foam were restricted to a maximum foam age at which the upper or lower limit of foam height still exceeded the fixed measurement heights. Furthermore, the distance between the fixed measuring positions and the milk/foam- and foam/air-interface is not constant.

In the following, the temporal and spatial changes of structural characteristic as well as rheological foam properties obtained for reconstituted milk will be discussed.

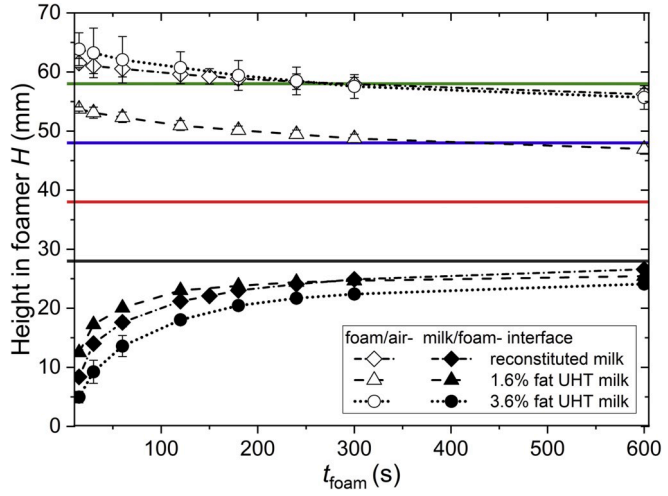

Fig. 5. Levels of milk/foam-interface (filled symbols) and foam/air-interface (open symbols) inside the foamer after whipping of reconstituted milk (diamonds), 1.6% fat UHT milk (triangles) and 3.6% UHT milk (circles) versus foam age t_{foam}. Dotted and dashed lines guide the eye. Positions of the measuring probes are displayed as solid lines.

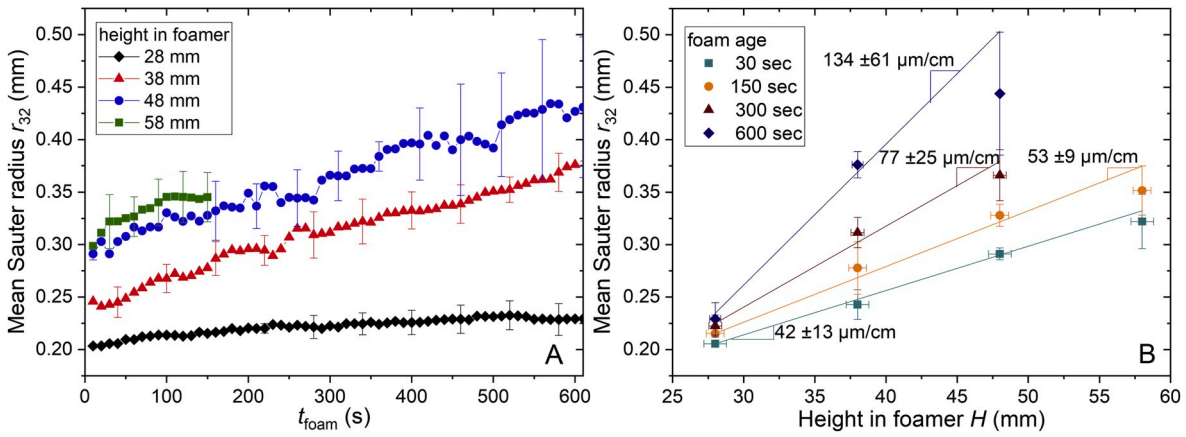

Fig. 6. Mean Sauter radius r_{32} of reconstituted milk foam versus foam age t_{foam} measured at four different heights inside the foaming device (A) and versus height inside the foam H at four different foam ages (B). Lines in B are linear fits to the data.

The mean radius r_{32} (Fig. 6A) varies initially between 200 µm and 300 µm, about double the bubble size of foams produced by steam injection (Jimenez-Junca et al., 2015, 2011), and monotonically increases over time. The average bubble size in foams was found to scale with the square root of foam age in previous studies (Durian et al., 1991; Lambert et al., 2010) as expected considering coarsening as a result of statistically-independent bubble coalescence events preserving the fractal structure of the foam. However, a linear increase of bubble size with the foam age, as seen here for milk foams, had been reported also for foams from β-lactoglobulin solutions (Rami-shojaei et al., 2009). The increase in mean radius is more pronounced in the upper regions of the foam in the present study and the slope dr_{32}/dt_{foam} varies between 3.7 µm/min at the bottom and 22 µm/min at the top of the foam. This difference may be attributed to more frequent bubble coalescence and enhanced Ostwald ripening due to thinner foam lamellae in the upper foam regions. Note, that no r_{32} data are available for the upper foam regions for long aging times due to an overall shrinkage of foam volume. Fig. 6B displays the change of r_{32} in axial direction. Bubble size always increases with increasing height in foam and this gradient increases over foam age, which is in good agreement with the bubble size growth versus height and time previously found in free drainage experiments (Vera and Durian, 2002).

As shown in Fig. 7, the width of the bubble size distribution as characterized by the span $= (d_{90}\text{-}d_{10})/d_{50}$ increases during foam aging, similar as the mean radius r_{32}. But no difference in span along the foam column height was observed above 28 mm height within the foamer. The spatial and temporal changes in bubble size documented here mainly characterize the coalescence process of a foam created from a certain type of milk using this particular whipping device.

Fig. 8A shows the evolution of the gas volume fraction φ at different heights within the column during foam aging. At all heights, a strong initial growth of φ is observed. In the upper regions of the foam, this turns into a weak linear increase at longer times. However, close to the bottom of the foam, $\varphi(t_{foam})$ goes through a maximum and then decreases and, at all times, the gas volume fraction remains below the critical gas volume fraction φ_c at which the maximum packing fraction of spherical bubbles is reached and they start to deform. For randomly packed monodisperse spheres $\varphi_c = 0.635$. This is a consequence of a rising liquid level underneath the foam due to drainage as schematically depicted in Fig. 5. As a consequence, the lowest measuring height in our setup here corresponds to the transition region between liquid and foam at long aging times. For the reconstituted milk foam investigated here, liquid fraction versus drainage time followed a power law $(1\text{-}\varphi) \propto t^n$ and the exponent n increases from −0.1 at 38 mm to −1.2 at 58 mm height within the foamer (data not shown). This latter result is in excellent agreement with earlier findings in free drainage experiments (Koehler et al., 2000) also reporting an exponent $n = -1.2$ at the foam top.

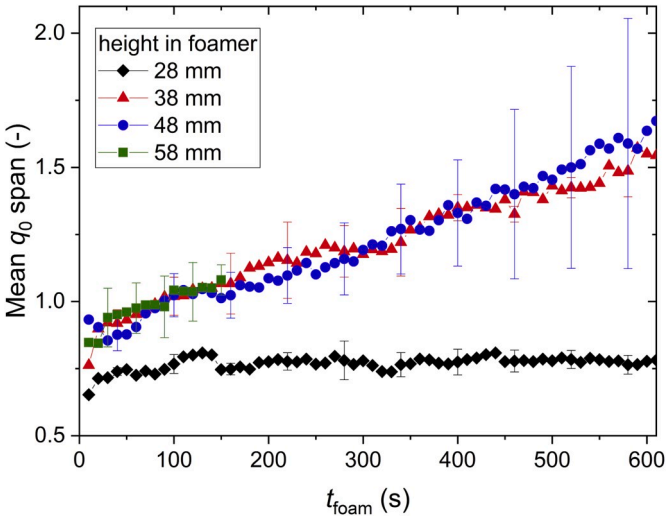

Fig. 7. Mean span $(d_{90}\text{-}d_{10})/d_{50}$ of the q_0 bubble size distribution of reconstituted milk foam versus foam age t_{foam} measured at four different heights inside the foaming device.

At any time, the gas volume fraction φ increases linearly with the height within the foamer H (Fig. 8B) and the gradient tends to increase with increasing foam age, i.e. the relative, drainage-induced change of gas volume fraction is more pronounced in the upper regions of the foam. Qualitatively, these results can be attributed to foam drainage. The quantitative changes of φ with time and/or height within the foam column characterize the drainage process in a foam created from this type of milk using this particular whipping device. Regimes of linear dependency of liquid fraction $(1\text{-}\varphi)$ on height within foams had been found previously in free drainage experiments (Saint-Jalmes and Langevin, 2002) in accordance with the solution of a simplified version of the free drainage differential equation (Verbist et al., 1996).

The yield stress of foams σ_y in general scales linearly within the Laplace pressure inside the bubbles Γ/r_{32} (Princen and Kiss, 1989) and quadratically with φ (Mason et al., 1996) yielding the following empirical model:

$$\sigma_y = k\ \Gamma/r_{32}\ (\varphi - \varphi_c)^2 \tag{6}$$

When φ_c is exceeded, gas bubbles start to deform and a yield stress emerges. Mason et al. (1996) found a numerical pre-factor $k = 0.51$. The temporal and spatial changes in σ_y for the investigated foam from

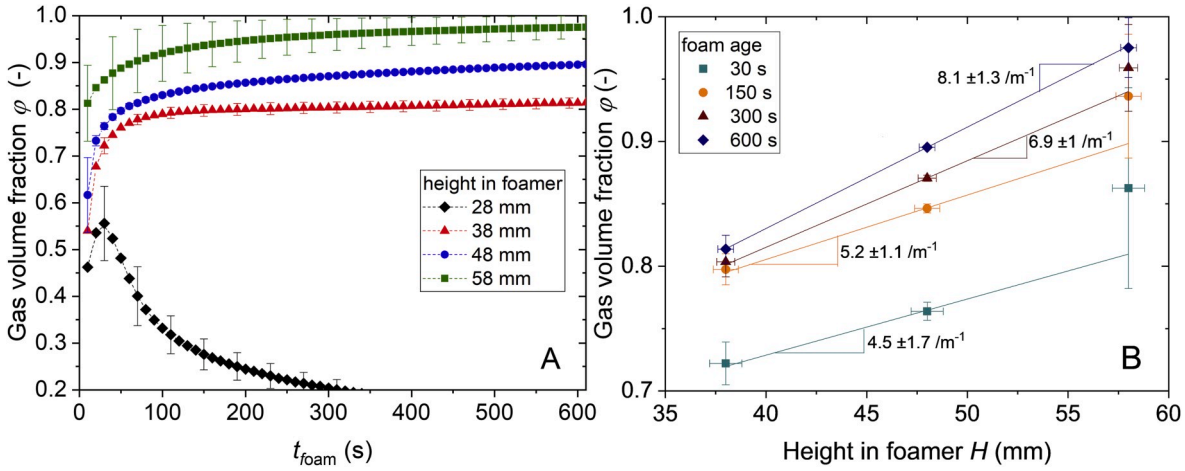

Fig. 8. Gas volume fraction φ of reconstituted milk foams versus foam age t_{foam} measured at different heights inside the foamer as well as determined volumetrically (A) and versus height inside the foamer H at different foam ages (B). Lines in B are linear fits to the data.

reconstituted milk are shown in Fig. 9A and B. The yield stress monotonically increases over time and absolute values between 1 and 15 Pa were obtained. Similar yield stress increase between 5 and 10 Pa had been reported for milk foam produced with steam injection (Jimenez-Junca et al., 2011). The initial increase in σ_y is less pronounced than expected from the increase in φ since the increase of σ_y with φ is partly compensated by the increasing r_{32}. At least qualitatively, the observed changes in σ_y correspond to the changes in φ and r_{32} discussed above. The increase of yield stress σ_y with the height in the foamer H is linear within the range of vertical distance investigated here. The increase of yield stress gradient with foam age is a consequence of the increasing gradient in φ.

Rheological and microstructural results obtained in situ for different types of milk are compared in terms of the time dependence of the r_{32}, φ and σ_y gradients along the vertical axis as shown in Fig. 10A–C. The change in r_{32} along the foam column axis (Fig. 10A) exhibits a similar linear increase with aging time t_{foam} for all three milk types. The absolute value of the gradient for the foam made from reconstituted milk seems to be systematically higher than for the other foams. The differences among the different milk types, however, are less pronounced than the changes over time. The gradient in gas volume fraction φ is significantly higher for the reconstituted milk than for the UHT milk types (Fig. 10B), which both exhibit similar gradients irrespective of foam age. It should be noted that this gradient refers to the upper part of the foam, the gas volume fraction at the lowest measuring position were mostly below φ_c, and thus not included in the gradient calculations. This gradient increases approximately linearly with foam age t_{foam} and the slopes are similar for all investigated foams. Such an increase of the gas volume fraction gradient with time at the lower end of a foam column is also predicted from free drainage theory (Verbist et al., 1996). The larger heterogeneity of bubble size and gas volume fraction in the foam from the reconstituted milk might be due to incomplete protein solubilization and thus lower availability for stabilization of foam lamellae during air entrainment. Foams consisting of larger bubbles possess lower interfacial area to be stabilized. If the protein concentration does not provide saturation of the interfacial area in a foam consisting of small bubbles, bubbles quickly coalesce and the average size increases (Lech et al., 2016). Subsequently, the coupling of bubble size and drainage velocity leads to the stronger gradients in the direction of gravity. Enhancing the protein solubilization by adding a second heating and mixing cycle during preparation of the reconstituted milk consequently led to 20% smaller initial mean bubble radius in the foams (data not shown).

The time evolution of the yield stress gradient along the vertical axis of the foam columns of different milk types is shown in Fig. 10C. This gradient increases monotonically over time and the increase is most pronounced within the first 3 min of foam age similar for all milk types.

Consistent with the finding that the gradients in φ and r_{32} are similar for the foams made from 1.6% to 3.6% fat milk we find similar absolute values for the yield stress gradient in these foams. For the reconstituted milk, the different gradients in φ and r_{32} compensate and consistently the yield stress gradient is similar to that of the other two types of milk foam.

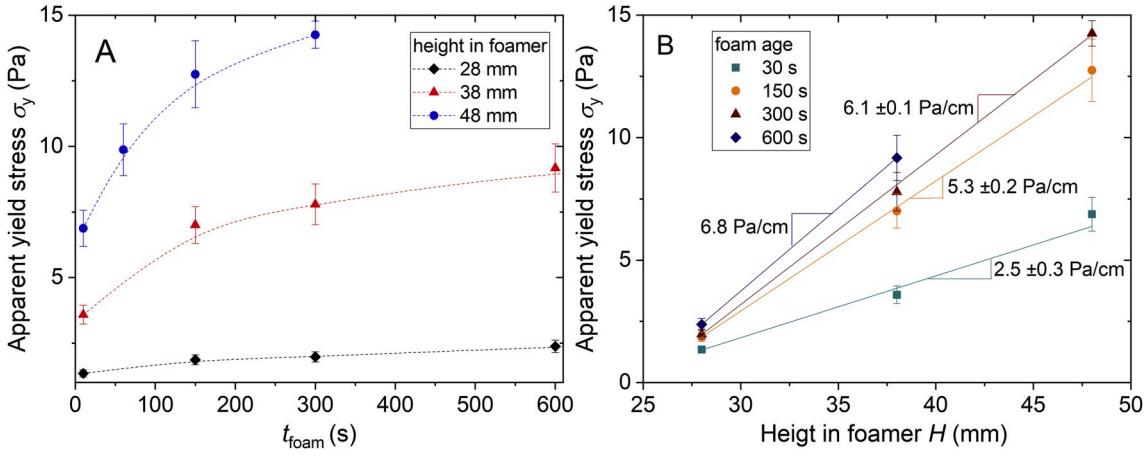

Fig. 9. Apparent yield stress σ_y of reconstituted milk foams versus foam age t_{foam} measured at different heights inside the foamer (A) and versus height inside the foam at different foam ages (B). Lines in A guide the eye. Lines in B are linear fits to the data.

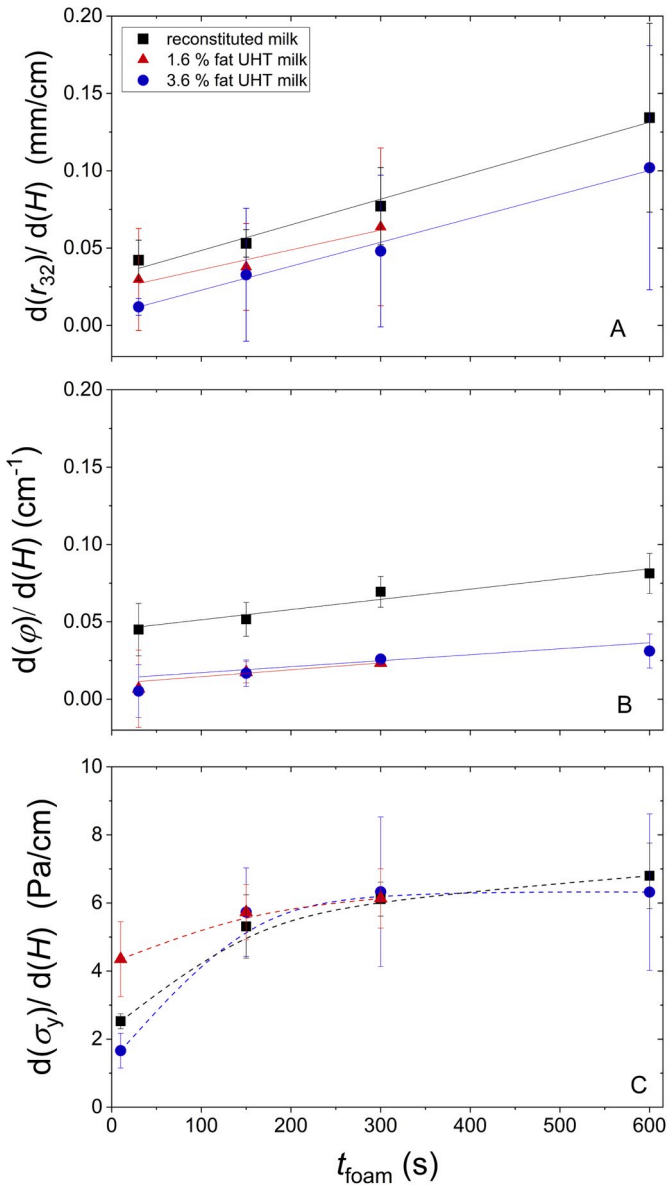

Fig. 10. Vertical gradient of Sauter radius $d(r_{32})/d(H)$ (A), gas volume fraction $d(\varphi)/d(H)$ (B) and yield stress $d(\sigma_y)/d(H)$ (C) of foams made from 1.6% to 3.6% fat UHT milk, and reconstituted milk versus foam age t_{foam}. Lines in A and B are linear fits to the data. Lines in C guide the eye.

We have analyzed all σ_y data obtained at different times, positions within the foams, and milk types in terms of the scaling suggested in Eq. (6). The Γ, r_{32} and φ data were directly taken from the corresponding measurements described above. The critical gas volume fraction φ_c was set to 0.635.

Fig. 11 shows the scaling of $\sigma_y/\Gamma/r_{32}$ with $(\varphi\text{-}\varphi_c)^2$ for all collected data. Despite some scatter in the experimental data, Eq. (6) describes the yielding of the foam types investigated here very well.

4. Conclusion

Here we presented the first apparatus combining foam generation and in-situ characterization of bubble size distribution and yield stress with simultaneous gas volume fraction measurement. The endoscopic setup and the fast, automated bubble size distribution analysis enable data collection with a spatial resolution on the order of millimeters and temporal resolution on the order of seconds. The temporal and spatial resolution of the yield stress measurement is restricted by a measuring

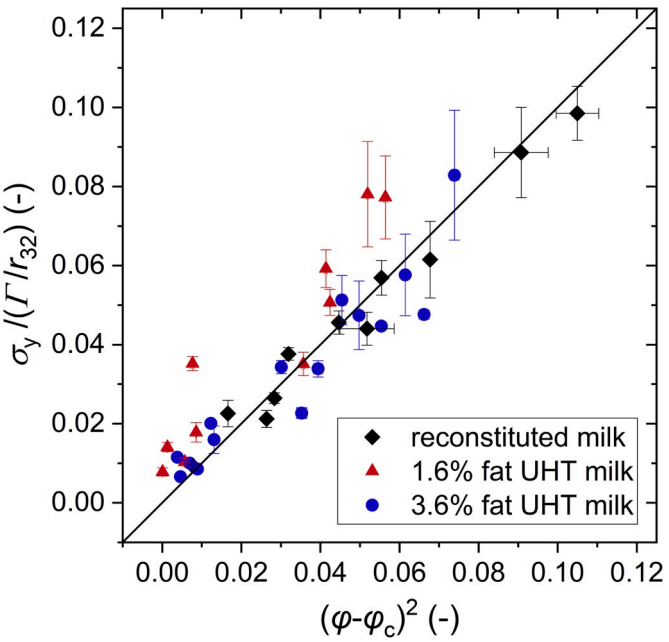

Fig. 11. Yield stress σ_y normalized by Laplace pressure Γ/r_{32} versus $(\varphi\text{-}\varphi_c)^2$ where φ_c is the critical packing fraction at which gas bubbles start to deform, here set to 0.635 corresponding to the random close packing of monodisperse spheres. Data are shown for foams of UHT milk with 3.6% and 1.6% fat, respectively, and reconstituted milk. Line shows the identity function.

time of 60 s and the vane rotor height of 9 mm. The gas volume fraction measurement follows the spatial resolution of the vane rotor. The apparatus was proven to resolve significant differences between foams from milk types that underwent different processing.

For the first time, yield stress profiles along the direction of drainage in foams were resolved. The yield stress increased with the height in the foam column as well as with ongoing foam drainage due to the increase in gas volume fraction, which was partially compensated by the bubble growth. The obtained milk foam yield stress values σ_y were found to scale with the product Γ/r_{32} $(\varphi\text{-}\varphi_c)^2$ as suggested by the phenomenological model of Mason et al. (1996), emphasizing the reliability of the measurement setup.

The new device allows for systematic studies regarding the effect of foaming parameters such as heating rate, temperature distribution within the cell or coil dimensions and speed on rheology and microstructure of created foams. Moreover, it offers new opportunities for fast characterization of new foam formulations, e.g. based on dairy products or milk substitutes, and their evaluation in comparison to regular milk foam.

Credit author statement

Annika R. Völp: experiment planning, construction of setup, experimental validation of setup, experiment realization, data processing, visualization and interpretation of results, documentation and reporting, paper writing, Lisa Kagerbauer: experimental realization, data processing, Jan Engmann: definition of objectives, planning setup and experiments, discussion of results, scientific advice, Deniz Z. Gunez: definition of objectives, planning setup and experiments, discussion of results, scientific advice, Cécile Gehin-Deval: definition of objectives, planning setup and experiments, discussion of results, scientific advice, Norbert Willenbacher: definition of objectives, planning setup and experiments, scientific advice, paper writing.

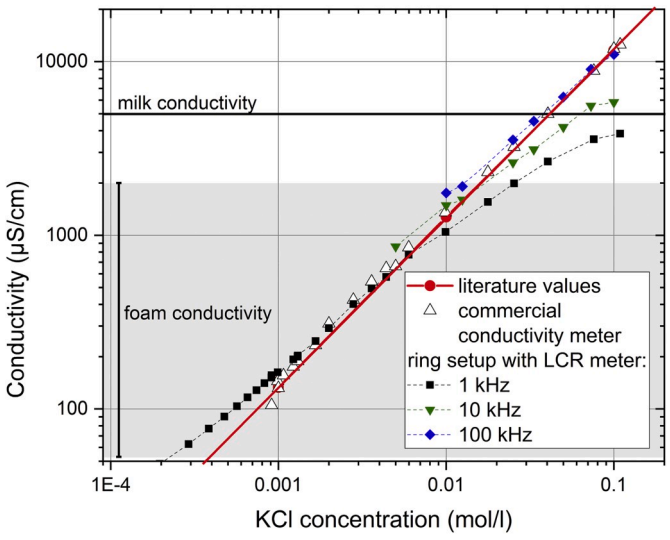

Fig. A1. Conductivity of potassium chloride solutions versus salt concentration measured with a commercial rod electrode connected to a conductivity meter (Inlab® 738 ISM and S230 seven compact, Mettler Toledo, Schwerzenbach, Schweiz) (hollow triangles) and brass ring electrodes inside the foamer connected to an LCR meter (U1733C 20,000-Count-Display Handheld LCR Meter, Keysight Technologies, Santa Rosa, USA) at frequencies of 1 Hz (black squares), 10 kHz (green triangles) and 100 kHz (blue diamonds). Solid red line shows the linear fit to the literature values (Pratt, Kenneth W. et al. "Molality-based primary standards of electrolytic conductivity (IUPAC Technical Report)." Pure and applied chemistry 73.11 (2001): 1783–1793.).

References

AMA Marketing, n.d. Welche der folgenden Kaffeearten bestellen Sie im Kaffeehaus/im Restaurant am liebsten? [WWW Document]. Stat. - Das Stat..

Cohen-Addad, S., Höhler, R., 2014. Rheology of foams and highly concentrated emulsions. Curr. Opin. Colloid Interface Sci. 19, 536–548. https://doi.org/10.1016/0021-9797(89)90396-2.

Durian, D.J., Weitz, D.A., Pine, D.J., 1991. Scaling behavior in shaving cream. Phys. Rev. A 44, 7902–7906.

Farr, R.S., Groot, R.D., 2009. Close packing density of polydisperse hard spheres. J. Chem. Phys. 131 https://doi.org/10.1063/1.3276799.

Feitosa, K., Marze, S., Saint-Jalmes, A., Durian, D.J.J., 2005. Electrical conductivity of dispersions: from dry foams to dilute suspensions. J. Phys. Condens. Matter 17, 6301. https://doi.org/10.1088/0953-8984/17/41/001.

Gunes, D.Z., Engmann, J., Gehin-Delval, C., Schmitt, C.L.M.E., 2018. Foams in food. In: Foam Films and Foams: Fundamentals and Applications. CRC Press, Boca Raton. https://doi.org/10.1201/9781351117746.

CO, n.d. Konsum von Kaffee in ausgewählten Ländern weltweit in den Jahren 2012/13 bis 2016/17 (in 1.000 Säcken à 60 Kilogramm). [WWW Document]. Stat. - Das Stat..

Jimenez-Junca, C., Sher, A., Gumy, J.C., Niranjan, K., 2015. Production of milk foams by steam injection: the effects of steam pressure and nozzle design. J. Food Eng. 166, 247–254. https://doi.org/10.1016/j.jfoodeng.2015.05.035.

Jimenez-Junca, C.A., Gumy, J.C., Sher, A., Niranjan, K., 2011. Rheology of milk foams produced by steam injection. J. Food Sci. 76, 569–575. https://doi.org/10.1111/j.1750-3841.2011.02387.x.

Koehler, S.A., Hilgenfeldt, S., Stone, H.A., 2000. Generalized view of foam drainage: experiment and theory. Langmuir 16, 6327–6341. https://doi.org/10.1021/la9913147.

Lambert, J., Mokso, R., Cantat, I., Cloetens, P., Glazier, J.A., Graner, F., Delannay, R., 2010. Coarsening foams robustly reach a self-similar trowth regime. Phys. Rev. Lett. 104, 1–4. https://doi.org/10.1103/PhysRevLett.104.248304.

Lech, F.J., Delahaije, R.J.B.M., Meinders, M.B.J., Gruppen, H., Wierenga, P.A., 2016. Identification of critical concentrations determining foam ability and stability of β-lactoglobulin. Food Hydrocolloids. https://doi.org/10.1016/j.foodhyd.2016.01.005.

Lexis, M., Willenbacher, N., 2014. Colloids and Surfaces A: physicochemical and Engineering Aspects Yield stress and elasticity of aqueous foams from protein and surfactant solutions – the role of continuous phase viscosity and interfacial properties. Colloids Surfaces A Physicochem. Eng. Asp. 459, 177–185. https://doi.org/10.1016/j.colsurfa.2014.06.030.

Lexis, Meike, Willenbacher, N., 2014. Relating foam and interfacial rheological properties of β-lactoglobulin solutions. Soft Matter 10, 9626–9636. https://doi.org/10.1039/C4SM01972E.

Lykema, J., Fleer, G.J., Kleijn, J.M., Leermakers, F.A.M., Norde, W., Van Vliet, T., 2000. Fundamentals of Interface and Colloid Science, Liquid–Fluid Interfaces. Academic Press.

Marze, S.P.L., Saint-Jalmes, A., Langevin, D., 2005. Protein and surfactant foams: linear rheology and dilatancy effect. In: Colloids and Surfaces A: Physicochemical and Engineering Aspects, pp. 121–128. https://doi.org/10.1016/j.colsurfa.2005.01.014.

Mason, T.G., Bibette, J., Weitz, D.a., 1996. Yielding and flow of monodisperse emulsions. J. Colloid Interface Sci. 179, 439–448. https://doi.org/10.1006/jcis.1996.0235.

Princen, H.M., Kiss, A.D., 1989. Rheology of foams and highly concentrated emulsions. IV. An experimental study of the shear viscosity and yield stress of concentrated emulsions. J. Colloid Interface Sci. 128, 176–187. https://doi.org/10.1016/0021-9797(89)90396-2.

Rami-shojaei, S., Vachier, C., Schmitt, C., 2009. Automatic analysis of 2D foam sequences: application to the characterization of aqueous proteins foams stability. Image Vis Comput. 27, 609–622. https://doi.org/10.1016/j.imavis.2008.10.004.

Saint-Jalmes, A., Durian, D.J., 1999. Vanishing elasticity for wet foams: equivalence with emulsions and role of polydispersity. J. Rheol. (N. Y. N. Y). 43, 1411–1422. https://doi.org/10.1122/1.551052.

Saint-Jalmes, A., Langevin, D., 2002. Time evolution of aqueous foams: drainage and coarsening. J. Phys. Condens. Matter 14, 9397–9412. https://doi.org/10.1088/0953-8984/14/40/325.

Statista, n.d. Was für Kaffee trinken Sie normalerweise auswärts, also z.B. im Café, im Restaurant oder unterwegs? [WWW Document]. Stat. - Das Stat..

Vera, M.U., Durian, D.J., 2002. Enhanced drainage and coarsening in aqueous foams. Phys. Rev. Lett. 88, 4. https://doi.org/10.1103/PhysRevLett.88.088304.

Verbist, G.D., Weaire, D., Kraynik, A.M., 1996. The foam drainage equation. J. Phys. Condens. Matter 8, 3715–3731. https://doi.org/10.1088/0953-8984/8/21/002.

Willenbacher, N., Lexis, M., 2018. Rheology of foams. In: Foam Films and Foams: Fundamentals and Applications. CRC Press, Boca Raton. https://doi.org/10.1201/9781351117746.

Worldpanel, K., n.d. UK's Favorite Coffee Drinks, Sales, Year Ending 25 February 2018 [WWW Document]. bbc NEWS..

Zhang, H., 2007. In: Barbosa-Cánovas, G.V. (Ed.), Electrical Properties of Foods. EOLSS, New York, USA, pp. 110–119.